Construction and Building Materials 35 (2012) 183–190

Contents lists available at SciVerse ScienceDirect

Construction and Building Materials

journal homepage: www.elsevier.com/locate/conbuildmat

Effect of wave distortion on acoustic emission characterization of cementitious materials

D.G. Aggelis *, A.C. Mpalaskas, D. Ntalakas, T.E. Matikas

Department of Materials Science and Engineering, University of Ioannina, 45110 Ioannina, Greece

ARTICLE INFO

Article history:
Received 6 December 2011
Received in revised form 23 March 2012
Accepted 26 March 2012

Keywords:
Fracture mode
Frequency
Rise time
Dispersion
Propagation distance

ABSTRACT

The fracturing behavior of materials can be nondestructively monitored by the acoustic emission (AE) technique, using sensors that detect the transient elastic waves after any crack propagation event. In addition to the information relatively to the total activity and the location of the cracks, certain waveform features supply detailed information on the type of cracking. The waveform of the emitted AE signal depends on the relative motion of the crack sides and therefore, it carries information on the mode of cracks. Therefore, AE is used for classification of the active cracking mode. This enables characterization of the current fracturing condition within the material and warning before final failure. Tension-related cracks, which in most materials and loading conditions are nucleated first, emit signals with higher frequency content and shorter rising time than shear cracks. However, in most cases wave propagation from the crack to the sensor is attenuative and dispersive. This results in signal distortion which is enhanced by geometry restrictions and material or damage-induced inhomogeneity. This results in strong change of the waveform shape and the calculated AE parameters. This effect is stronger as the propagation distance increases rendering crack classification troublesome for structures where the separation distance between sensors is long. In the present study, fracture experiments were conducted in cementitious specimens in order to investigate the influence of distance on the AE parameters as measured by sensors at different distances from the source. Numerical simulations based on the finite difference method are also used to enlighten the problem and expand to different material conditions. This is one of the first studies of wave dispersion examined not from the classical ultrasonics point of view of phase velocity dependence on frequency but from the AE view, where specific waveform parameters are of interest. Experimental and numerical results show that the influence of the propagation path is crucial and should be taken into consideration for AE characterization of large structures, while it should not be neglected even in small-scale laboratory studies in order to improve crack characterization.

1. Introduction

Acoustic emission (AE) is a nondestructive inspection technique utilizing the transient elastic energy which results mainly from crack propagation events inside a material [1,2]. The dislocation created at the tip of the crack excites elastic waves which propagate outwards and can be captured by sensors on the surface of the material. Acoustic emission is studied in relation with the damage evolution under dynamic loading or relatively to crack propagation rate [3–5]. It is reasonable that the number of recorded signals during loading can be correlated with the actual number of active cracks within the material [6,7]. For certain structures, the rate of incoming activity is a stand-alone criterion on which engineering decisions are based concerning safety, while strict standardization has been applied internationally. Apart from the cumulative AE activity, each signal carries raw information from its source, concerning the severity (the amount of displacement of the crack sides under the specific load) and the mode of fracture (opposing movement of the crack sides or parallel). Therefore, the qualitative characteristics of the waveform, like the amplitude, duration and main frequency may reveal crucial information on the damage mode and fracture intensity inside a material [8,9]. The main benefit of this approach is based on the fact that for most materials and loading conditions, shear types of failure follow tensile [10,11]; therefore, the classification of cracks according to their mode would indicate the current fracturing stage and provide an early warning of final failure. Controlled laboratory studies in different material systems shed light into the correlation of AE characteristics with the cracking mode. The connection between the mode of crack and the wave recorded at a specific point is a very complicated subject depending on the motion of the crack tip, as well as to geometry factors like orientation of the crack relatively

* Corresponding author. Tel.: +30 26510 08006; fax: +30 26510 08054.
E-mail address: daggelis@cc.uoi.gr (D.G. Aggelis).

0950-0618/$ - see front matter © 2012 Elsevier Ltd. All rights reserved.
http://dx.doi.org/10.1016/j.conbuildmat.2012.03.013

to the receiver and propagation distance. While the present experimental and numerical study aims to enlighten aspects of the problem, some simple remarks concerning the excited wave modes can be stated. When a dislocation occurs inside a material, both modes of bulk waves (longitudinal and shear) are reasonable to be emitted. However, it is also reasonable that a tensile (or mode I) cracking incident excites a large part of the elastic energy in the form of longitudinal waves, due to the transient volumetric change near the vicinity of the crack tip. On the contrary, when shear cracking develops, the percentage of energy is shifted in favor of the shear waves due to the shape distortion that shear action induces in the vicinity of the crack tip. In the first case, the main energy carrier is also the fastest wave type leading to waveforms with short rise time (RT), see Fig. 1, top. RT is the delay between the onset of the waveform (practically the first threshold crossing) and the moment of peak amplitude. Correspondingly, the rise angle of the waveform is high, as calculated by the Amplitude, A over RT. Recently in the field of concrete, the inverse of the rising angle is studied, namely RA in μs/V [10]. In the case of shear incident, the main part of energy travels with the shear waves which are slower, leading to longer RT and lower rise angle, (see Fig. 1, bottom). The validity of these general remarks is very sensitive to geometric conditions, relative orientation and the propagation characteristics of the medium, as will be discussed in the text. However, these assumptions have been examined in several experimental studies. Although a literature review on the subject is not within the scope of this paper, some main points are introduced in this section in order to establish the parameters that are measured and discussed throughout the text. The AE waveform parameters which have been correlated with the fracture mode are mainly the RA value and the frequency content expressed by the number of threshold crossings over the duration of the waveform (average frequency, AF) [10]. It has been found that the RA value increases, while the average frequency decreases as damage is being accumulated in bending experiments in steel- and vinyl-fiber reinforced concrete [12,13]. Additionally, these parameters undergo a great change at the moment of the main crack formation, which indicates the shift of the dominant failure mechanism from matrix cracking to fiber pull-out [14,15]. This kind of analysis has also proven useful in rock failure [16], fracture of composite laminates [17–19] which exhibit matrix cracking (mode I) and delaminations (mode II), corrosion cracking in concrete [20] and damage evaluation on reinforced concrete panels subjected to seismic load [21]. The mutual trend in all studies is that despite differences in material, propagation path length or specimen size, the shear type of damage usually results in waveforms with longer rise time, duration, high RA and lower frequency than tensile.

The shifting trends of these parameters during fracture in concrete have been proven quite reliable in several laboratory studies. Consequently, classification of AE signals concerning the mode of the original crack has proven quite successful, based on AE parameters like AF and RA [15,20,22]. However, the application of the same laboratory criteria to real structures is not straightforward. This is mainly due to intrinsic problems that usually hinder the exploitation of this kind of information. Some of the factors complicating the assessment are the specimen or structure's size and geometry, the heterogeneity of the material and the sensor's response as explicitly explained in [19]. These factors render the results case-specific and prevent from general application, especially when the goal is other than simply crack location. As a consequence, any attempt of AE material characterization, would greatly benefit by the complementary study of the influence of the propagation path on the signal acquired at different surface measurement points. In this study cementitious mortar specimens were fractured under bending while their AE activity was monitored by two sensors. The sensors were placed at different distances from the notch which enabled acquiring the transient wave from the same fracturing event at two distinct points and evaluating the effect of distortion and attenuation based on the separation distance. The problem was also numerically simulated by an available finite differences code, which gave the opportunity to include different contents of simulated cracks and to expand to frequencies other than the experimental. The numerical and experimental results show that the effect of waveform distortion is strong and it should not be neglected in laboratory. Furthermore, it should certainly be taken into consideration in situ in order to expand the use of simple crack classification schemes to real structures.

It is mentioned that the acquired experimental and numerical waveforms were analyzed for their acoustic emission parameters. Therefore, the analysis is not based on a typical ultrasonic approach, which usually employs calculations of wave speed and attenuation. The investigation involves parameters of the AE waveforms, like RT, RA and AF, which although carry information on the mode of the cracking event they suffer strong changes due to propagation through an inhomogeneous medium like concrete. This discussion is particularly important in the field of concrete where standardization is currently attempted [10], while it also applies in thin-walled structures due to plate wave dispersion [23,24].

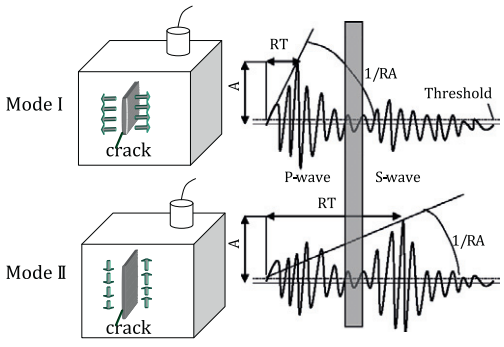

Fig. 1. Cracking modes and recorded AE waveforms.

2. Limitations for AE characterization

When the specimen's dimensions are finite, reflections from the edges interfere with the original AE waves. However, this is not the only complication met in AE measurements. Almost the total number of AE applications concern either piezoelectric sensors attached on the surface, or in some cases non-contact measurements, based on laser interferometry [25]; in both cases the information comes from the transient displacement of the surface. This introduces the effect of geometry even in large structures, when reflections from other sides are not expected. The reason is that as the primary wave front of the emitted AE signal impinges on the surface, mode conversion occurs and a Rayleigh wave is continuously excited. Since the propagation velocity of Rayleigh is lower, the shape of the pulse is automatically influenced, causing distortion and changing crucial waveform parameters like duration and rise time.

Apart from the waveform distortion caused by the differential velocity of the wave modes, excessive dispersion is caused depending on the heterogeneity of the material. It is mainly attributed to scattering which redirects the wave energy each time the wave front impinges on a scatterer [26]. Dispersion applies to inhomogeneous materials, like concrete [27–29], or other particulate and fiber composites [30,31] and suspensions [32] and is enhanced by the presence of damage in the form of micro-cracks and microstructure [33–35]. It is reasonable that the characteristics of a wave emitted by a crack are severely distorted while propagating through a heterogeneous system containing numerous other

cracks which act as scatterers. The interaction between the microstructure and the propagating elastic wave has been correlated to the damage degree and typical size, mainly through measurements of attenuation and phase velocity in the several ultrasonic studies [29,31,36]. It is reasonable that the effect of inhomogeneity on the transient AE signal (which is in fact an ultrasonic wave) is equally important. Therefore, the signal's shape and main characteristics, as quantified by AE analysis, also changes for different measurement locations. The evaluation of this distortion is the primary aim of this work.

3. Experimental details

Two different mortar mixtures were produced consisting of six specimens each. One was plain mortar (PM) and the other included 0.5% (vol.) of straight steel fibers (steel fiber reinforced mortar, SFRM). Their length was 25 mm, their diameter 0.6 mm, their density 7.85 kg/dm^3 and were supplied by CHIRCU PROD-IMPEX COMPANY SRL, Romania. The aggregates consisted of 100% crushed sand with maximum aggregate size 4.75 mm and fineness modulus 2.93, while water/cement ratio was 0.55 by mass. The density and the water absorption of the sand were 2500 kg/m^3 and 2.44% respectively. The exact mix proportions were as follows: cement type II 440 kg/m^3, water 242 kg/m^3, sand 1529 kg/m^3, super-plasticizer 4.5 kg/m^3. For the fiber reinforced mortar the mix proportions were the same with the addition of 39.3 kg/m^3 of steel fibers and modification of sand amount to 1517 kg/m^3. The specimens were cured in water for 28 days prior to testing.

The specimens were 40 × 40 × 160 mm in size. They were subjected to three-point bending according to EN 13892-2:2002 [37] (Fig. 2a). In order to secure that the crack would initiate at the center of the specimen a notch was created by inserting a small wooden stick in the midspan of the side to be placed at the bottom during bending (tensile side). The load was applied at a constant rate of 50 N/s until fracture and the loading was automatically terminated at the moment of load drop. As to AE monitoring, two AE sensors (Pico, PAC) were attached to the side of the specimen as seen in Fig. 2b. They are considered quite broadband with central frequency of 500 kHz. Roller bearing grease was used for acoustic coupling, while the sensors were secured by the use of tape during the experiment (see Fig. 2b). The horizontal distance between the sensors was 40 mm and the first was placed at the horizontal distance of 15 mm from the notch, as seen in Fig. 2b. The signals were recorded in a two-channel monitoring board PCI-2, PAC with a sampling rate of 5 MHz. The threshold was set to 40 dB in order to avoid ambient noise and the acquired signals were pre-amplified by 40 dB.

4. Results

4.1. Total activity

The small size of the specimen results in relatively small level of AE activity. Typical graphs of cumulative AE activity for PM and SFRM are depicted in Fig. 3a and b respectively. The activity of each sensor (S1 near the crack, and S2 away from the crack) is presented separately. The number of signals is generally less than 100 in total and the population is divided almost evenly in both receivers. This shows that despite the inherent attenuation, that will also be discussed later, the small separation distance enables capturing the fracture events by both sensors. The largest percentage of AE hits is received at the end of the experiment indicating that serious cracking processes take place only at the latest stages of loading, just before the maximum load has been reached. The almost vertical increase of the AE activity at the moment of fracture is preceded by small number of few signals approximately 2 s before final fracture, most likely due to fast-developing micro-cracking just before final failure.

It is interesting to observe qualitative characteristics of the AE waveforms as captured by the two receivers. Fig. 4 shows the time histories of AF of the AE signals of the same specimens as recorded by the two sensors separately. The symbols represent the AF of each signal, while the lines stand for the moving average of the recent 5 hits in order to demonstrate the trends more clearly. For both cases, after some fluctuations, AF is decreased at the moment of final failure, which is typical for cementitious materials [10,12,14,38]. Although the differences in average values are discussed in the next section, it is evident that generally S1 records signals with higher AF than S2 (see Fig. 4a). The same holds for the case of Fig. 4b for a typical SFRM specimen. Additionally, in the case of SFRM the frequency indicator is in general at lower level compared to plain mortar, which will be discussed along with the average results. Fig. 5, shows the time history of RA for the same specimens. In both cases, RA increases sharply just before the termination of the experiment as is typical for materials at the onset of macrofracture [10,38]. For the plain mortar the initial RA values are below 1 ms/V, while as main fracture approaches, values higher than 10 ms/V are depicted. Again a distinct difference is seen between the two sensors, with the sensor closest to the crack (S1)

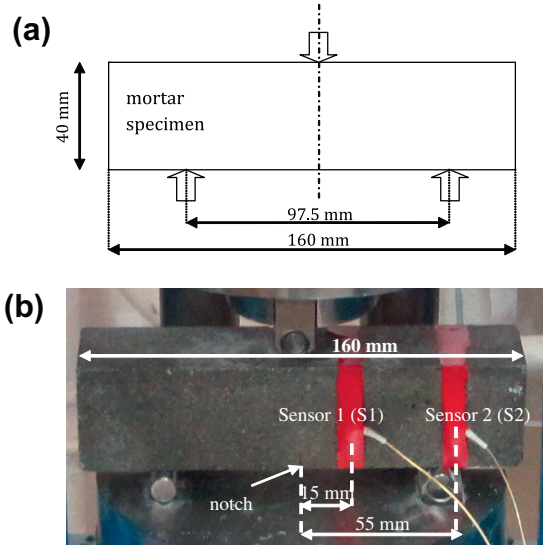

Fig. 2. (a) Schematic representation of three point bending test and (b) photo of the specimen with AE sensors.

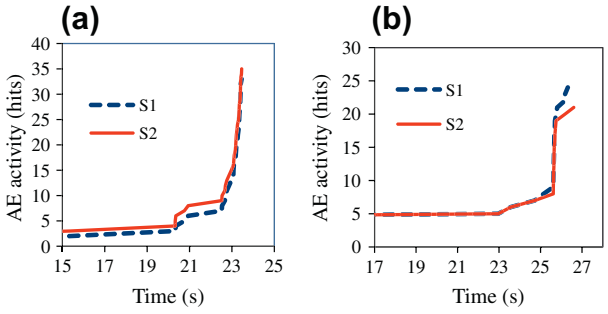

Fig. 3. Typical cumulative AE activity of (a) PM and (b) SFRM.

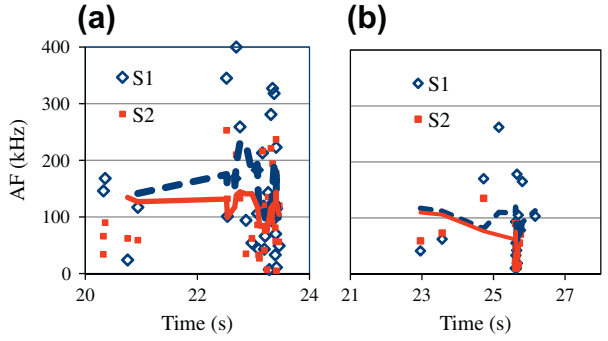

Fig. 4. AF history for typical (a) PM and (b) SFRM specimen as obtained by the two sensors.

exhibiting lower values for both specimens. Correspondingly, in this case SFRM exhibits higher RA than PM, which is again attributed to the fiber action as was the behavior in AF.

4.2. AE events

The above indicative curves are based on the total number of signals received by each sensor, including any possible source, even though it is reasonable that the main source is the notch at the center. Although the trends would still be clear, in order to exclude any random signals, the data were strictly limited to the "AE events". An AE event is the source incidence that releases elastic energy and is captured by both receivers within a short time window. This secures that each signal recorded by the first receiver can be compared to the same source signal as captured by the other receiver after traveling an additional propagation path. For each specimen, the values of the AE parameter recorded during failure by the first sensor were averaged and compared to the corresponding average value of the second sensor. Fig. 6a shows the average RA values as captured by the two sensors (S1 at horizontal distance of 15 mm and S2 at 55 mm from the notch). Each point typically represents the average of approximately 20 individual values which was a usual number of identified AE events during the bending test of a specimen. The symbols corresponding to each specimen are connected by a straight line, while the large symbols are the average of the individual points for each distance. The RA values captured from S1 are between 130 and 390 μs/V. For all the specimens there is an almost uniform increase in the RA for S2 (between 740 and 1010 μs/V). In average, the RA of the second receiver is increased by more than 3 times (901 μs/V) compared to the first (278 μs/V). This is a definite indication of distortion that occurs for the same signals, for the short additional propagation distance between S1 and S2. This indicates how important the propagation length is for AE analysis even in laboratory scale. Fig. 6(b) shows the corresponding graph for SFRM. The trend is similar, with S2 exhibiting 1057 μs/V, almost three times higher than the RA of S1 (371 μs/V). Though distance is equally critical for these measurements as well, a slightly higher value of RA is exhibited for SFRM, while the variability seems much stronger.

The other basic feature of interest in crack classification schemes is AF which is a rough but very indicative expression of the frequency content, as explained in the introduction. It is generally well known that when a pulse propagates through an inhomogeneous medium its main frequency is downshifted [30,36], due to scattering. In each specific specimen, AF decreases between the first and second receiver. Results for plain mortar (Fig. 7a) and SFRM (Fig. 7b) share approximately similar trends for the average value of AF. The decrease is of the order of 20%. This change in the additional propagation of approximately 40 mm is indicative of attenuation and distortion mechanisms that can influence basic AE parameters even in laboratory scale.

Concerning the wave amplitude it is expected that energy-related parameters are downgraded as the wave propagates through cementitious material due to damping and scattering. Amplitude is a crucial parameter of the waveform. Not only because it is directly connected to the cracking intensity [7,8], but because it also influences most of the rest waveform parameters. Higher amplitude, results in larger number of oscillations above the threshold (counts), influencing therefore, the duration, RT, AF and most of the calculated AE features. This is of paramount importance in actual structures, where long distances impose severe attenuation in the signal. The exact results for both types of specimens are seen in Fig. 8a and b. For PM, the amplitude received by the nearest sensor is 58.4 dB in average. Inherent attenuation imposes a decrease of approximately 6 dB for the second receiver. For SFRM the decrease is 4 dB in average still as seen by Fig. 8 noticeable and repeatable decrease of amplitude is exhibited even in laboratory scale.

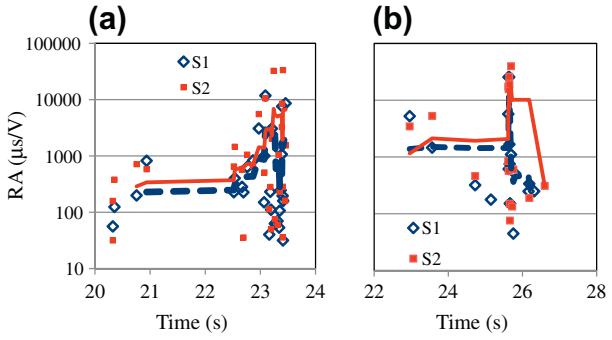

Fig. 5. RA history for typical (a) PM and (b) SFRM specimen as obtained by the two sensors.

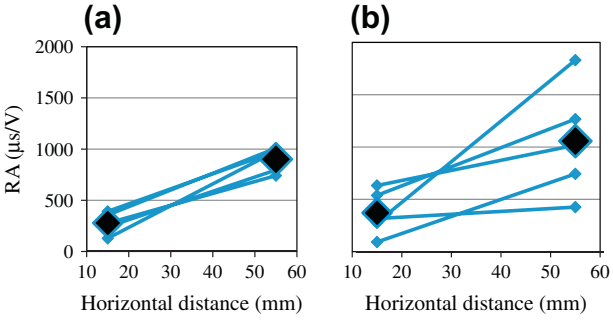

Fig. 6. RA values for all (a) PM and (b) SFRM specimens for two propagation distances. Small symbols represent average values for individual specimens while large symbols stand for the average of all corresponding points.

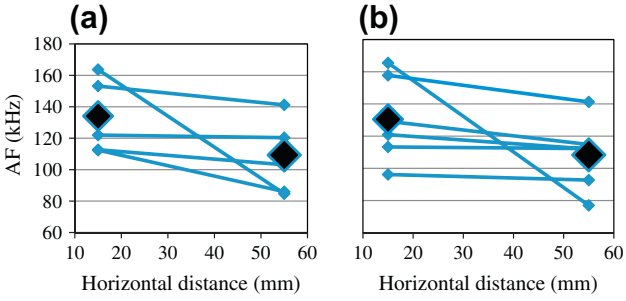

Fig. 7. AF values for all (a) PM and (b) SFRM specimens for two propagation distances. Small symbols represent average values for individual specimens while large symbols stand for the average of all corresponding points.

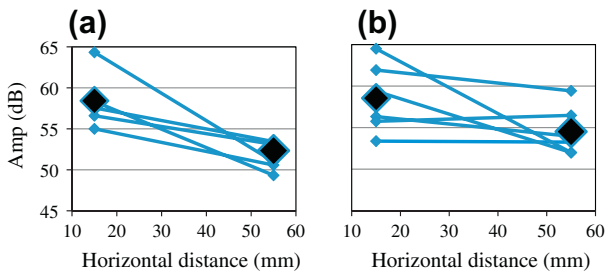

Fig. 8. Amplitude values for all (a) PM and (b) SFRM specimens for two propagation distances. Small symbols represent average values of individual specimens while large symbols stand for the average of all corresponding points.

5. Numerical simulations

5.1. Model

Numerical simulations are generally used in order to increase the understanding of wave propagation in specific problems. They enable recognition of wave modes and reflections in complicated geometries. Additionally, they can be used to expand to different geometries and cases that are not experimentally tested. In this case indicative two-dimensional simulations were conducted on the specific geometry of the experimental test including different cases of material texture, namely homogeneous (simulating cement paste), matrix with round scatterers (paste with sand grains, mortar), and three different contents of thin cracks. The fundamental equation governing the two-dimensional propagation of elastic waves in a perfectly elastic medium, is seen below:

$$\rho \frac{\partial^2 \underline{u}}{\partial t^2} = \mu \nabla^2 \underline{u} + (\lambda + \mu) \nabla \nabla \cdot \underline{u} \quad (1)$$

where $\underline{u} = u(x, y, t)$ is the time-varying displacement vector, ρ is the mass density, λ and μ are the first and second Lame constants respectively, while t is time. The simulations were conducted with commercially available software [39] that solves the above equation in time domain with the finite difference method in the plane strain case. Eq. (1) is solved with respect to the boundary conditions of the object, which include the input source that has pre-defined time-dependent displacements at a given location and a set of initial conditions [40]. For heterogeneous media, propagation in each distinct homogeneous phase is solved according to Eq. (1), while the continuity conditions for stresses and strains must be satisfied on the interfaces. In this case, the propagation of an elastic wave in mortar is simulated. The aim is mainly to study the influence of cracks and sand grains scattering on the propagating wave. Different excitation types could be used to create this transient wave, such as force, velocity or displacement. In cases of crack propagation, where a permanent dislocation occurs, the magnitude of crack displacement and the AE wave motion are commonly modeled [41]. Since the source of the elastic wave in this simulation is supposed to be a crack propagation event, a short displacement excitation was also used as a conventional way to excite the transient pulse.

The basic geometry of the model is shown in Fig. 9. The "source" is placed at the bottom of the mid span, at the position of the notch in the actual specimen with a length of 1 mm. It introduces one cycle of 500 kHz in the longitudinal mode. This frequency is the resonant frequency of the sensors used in the experimental section and was indicatively selected among many other possible values since in AE the major frequency is not known a priori. Two receiving sensors (S1 and S2) are placed in the middle of the height, with horizontal distance of 15 mm and 55 mm on the right side from the excitation point (see Fig. 9). The receivers are simulated by straight lines. In order to better simulate the experimental case their length was set to 5 mm which is the diameter of the specific AE transducers used. Considering the grid of 0.2 mm, the sensor length includes 25 nodes. The sensor's calculated response is the average of the displacement of these nodes either in the direction vertical to their length or parallel. Since, the experimental transducers record motion components vertical to their surface, the same response was also selected to be analyzed from the simulation results.

Materials were considered elastic without viscosity components. Different cases were simulated, namely homogeneous elastic matrix, matrix with 50% stiff elastic scatterers simulating sand grains, and matrix with sand grains and different contents of crack, namely 1%, 5% and 10% by cross section area. The properties of the different materials are seen in Table 1. The sand grains were simulated by circles of 1 mm diameter and the cracks by thin inclusions of size 0.5×2 mm assigned the properties of air. It is mentioned that the above described model is indicative of concrete-like materials and by no means is the only appropriate case for studying the problem in hand.

The focus, from the engineering point of view is given on simulating the actual geometry examined experimentally and not on the numerical method itself. However, certain prerequisites should be followed in order for the analysis to lead to reliable results. Concerning the mesh size, a preliminary evaluation took place to select a suitable value for accurate as well as time-efficient simulation. Different values of mesh size were applied, namely from 1 mm down to 0.1 mm and the corresponding wave flight times to the 2nd receiver were calculated. As the mesh became finer, the calculated transit time increased slightly, as seen in Fig. 10. This dependence seems quite linear and projecting the value of the linear fit for infinitesimally small grid, the transit time would be 15.627 μs. For grid of 0.2 mm, the result was 15.5156 μs, resulting in an error of 0.7% and in quite reasonable calculation time. Indeed, for a basic frequency of 500 kHz, the major wave length is about 8 mm resulting in 80 points per wave length. Concerning the time sampling, the time step was set at the value of 0.0182 μs. Considering that the basic period was 2 μs, it is clear that the number of

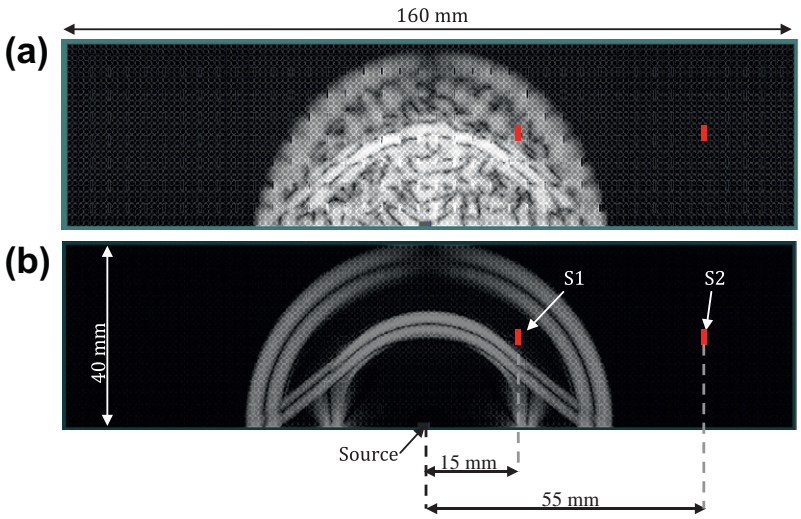

Fig. 9. Geometrical model and displacement field 10 μs after excitation for material with 50% sand grains and 5% cracks (a), and homogeneous matrix (b).

Table 1
Properties of the materials used for the simulation model.

Material	λ (GPa)	μ (GPa)	ρ (kg/m^3)	C_p (m/s)
Cement matrix	8.3	12.5	2100	3984
Sand grains	15.3	18.5	2600	4486
Air	10^{-4}	10^{-6}	1.2	316

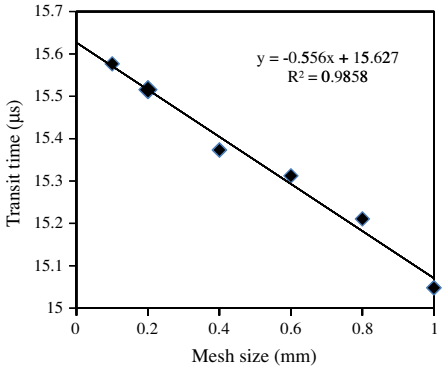

Fig. 10. Transit time between excitation point and the 2nd receiver of the model of Fig. 9 vs. mesh size.

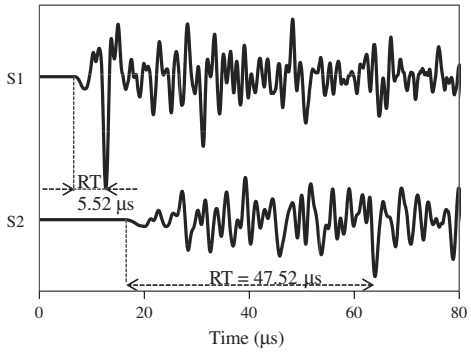

Fig. 11. Simulation waveforms for the two sensors for material with 50% grains and 5% crack content.

points representing one cycle are higher than 100, while in similar studies the numbers of 20 points per wavelength and cycle are considered adequate [42]. The total simulation time window was 100 μs.

5.2. Simulation results

Fig. 9a and b depict the displacement field at approximately 10 μs after excitation for the case of material with 50% grains and 5% cracks and for homogeneous material respectively. The distortion of the wave field is evident for the heterogeneous case and is accumulating as the wave propagates away from the excitation. The waveforms received by the two sensors for the first case are seen in Fig. 11. Despite the short initial excitation of one cycle, both sensors record a long waveform due to the multiple scattering of the wave on the several heterogeneities either in the form of grains or in the form of cracks. One of the distinct differences between the two waveforms concerns the rise time (the delay of the maximum peak compared to the onset). For S1, RT equals 5.5 μs, while for S2 the maximum peak delays considerably resulting in a RT of almost 48 μs. It is mentioned that the onset of the waveform was defined by the first threshold crossing, the threshold being 2% of the

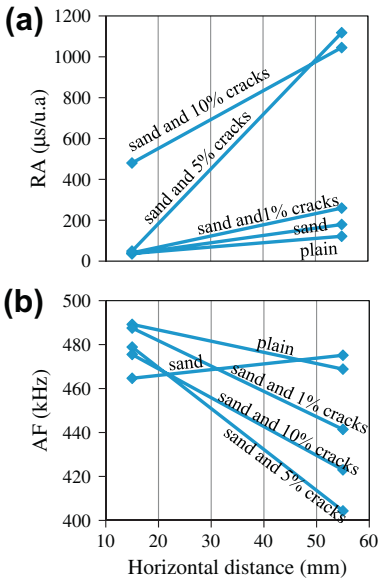

Fig. 12. RA (a) and AF (b) for the two sensors and different material conditions.

maximum amplitude of the waveform of S1, while 5% has also been checked without serious change in the resulting trends. Additionally, the oscillations are less dense in the case of S2, implying a downshift in the basic frequency. The exact values of RA and AF as measured from the simulation waveforms are presented in Fig. 12 for both receivers (S1 at 15 mm, S2 at 55 mm). Concerning RA (Fig. 12a) there is a certain increase for the second receiver, from three to six times between homogeneous material and material with 1% of cracks. For 5% cracks the increase for the 2nd receiver is explosive (23 times higher than the 1st sensor). Finally for 10% cracks the RA is quite high from the first receiver (480 μs/unit amplitude (u.a.)), showing the heavy influence of heterogeneity on the shape of the waveform. It is reminded that the RA of the excited pulse is 0.5 μs/u.a. (one fourth of the period of 2 μs over the unity excitation amplitude). Through the propagation distance of 58 mm, which is the straight distance between the excitation point and 2nd receiver, this value becomes approximately 2000 times higher (1045 μs/u.a.) due to distortion of the pulse on the cracks and aggregates. It is easily realized that the original information of the pulse is heavily masked and that any classification approach based on the waveform as received by the sensor would most likely be misleading.

Fig. 12b presents the values of AF. Since the basic frequency of the excitation is 500 kHz, reasonably the first sensor acquires frequencies close to the original pulse (465–490 kHz) for all cases. With the only exception of the geometry with sand grains, the frequency is downshifted for the second receiver in all the models. Especially for the cases of 5% and 10% cracks, AF decreases by 16% and 11% respectively. The above simulations confirm that even for such short distances of a few cm, the signal distortion is dominant owing only to elastic scattering excluding viscosity effects.

6. Discussion

The above experimental and numerical results taken from small geometries enable drawing of conclusions towards the improvement of signals classification schemes based on simple AE features. Table 2 summarizes the average values of basic AE parameters as experimentally measured by both sensors. The decrease of AF by almost 20% and the increase of RA by more than 3 times for the 2nd sensor (55 mm from the notch), shows that the position of

Table 2
Experimental AE parameters.

	Dist. from notch (mm)	AMP (dB)		RA (μs/V)		AF (kHz)	
		Aver.	St. dev. (%)	Aver.	St. dev. (%)	Aver.	St. dev. (%)
Plain	15 (Sensor 1)	58.4	5.0	278.4	33.2	134.1	14.8
	55 (Sensor 2)	52.3	4.5	900.7	12.2	109.3	18.5
SFRM	15 (Sensor 1)	58.5	6.5	371.2	51.9	130.5	18.6
	55 (Sensor 2)	54.5	4.9	1056.9	45.2	108.3	18.4

the sensors with respect to the crack location is crucial. The results, even in such close quarters include the effect of dissipation and scattering and differ significantly from the original pulse, as emitted by the source. Since the pulse suffers substantial changes for a short additional distance of 40 mm between the receivers, it is understandable that the effect in actual structures would be even stronger. In real-size structures, a finite number of sensors are placed in order to cover as large volume of the material as possible. Therefore, a cracking incidence may have its source just millimeters beneath the sensor or at a distance of several meters away. Although the signal may be acquired in both cases (provided that its energy is high enough), its characteristics should definitely differ at various measurement points. Therefore, the event location relatively to the sensor is crucial in order to evaluate how much the signal has been distorted while propagating. As already mentioned, in the engineering use of AE, crack characterization is important since it gives insight in the fracture stage. In laboratory scale, assuming that distortion and attenuation are limited, classification criteria have been studied based on specific values of RA and AF [15,22]. As an example from [15], tensile matrix cracking in steel fiber reinforced concrete under bending was characterized by an average AF of 400 kHz and RA less than 1 ms/V, while mixed-mode fracture (macro-cracking with fiber pull-out) by AF of 150 kHz and RA of 4 ms/V, as seen also in Fig. 13. This classification produced very accurate results (less than 1% overlapping points) in beam specimens of 400 mm length and sensors placed nominally 50 mm away from either side of the expected crack. However, if the same criteria were to be used in situ for different conditions and sensor separation distances, the classification would not necessarily be equally accurate. Under the light of the experimental results of the present study it is understood that the RA of a tensile event after propagation through a few cm of heterogeneous cementitious material would increase by about 3–4 times, as was seen in Table 2. Simulations at higher frequencies indicate a much stronger increase of RA (from five to twenty-five times depending on the material's condition). Similarly the frequency content would

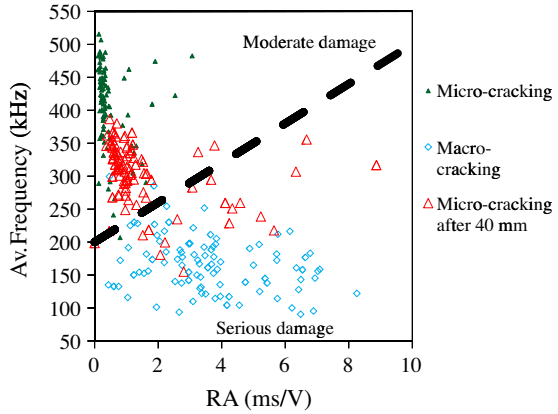

Fig. 13. Cracking mode classification for steel fiber reinforced concrete beams of 400 mm size under bending.

decrease by more than 20% for propagation of a few additional cm, as was seen in Fig. 7. When this distortion effect is incorporated in the values of the micro-cracking population of Fig. 13 (small solid green triangles) by multiplying the RA of each point by 3.5 and decreasing AF by 25%, the new set of data (larger open red triangles) it results in much stronger overlap with the original macro-cracking (20% of the population). Therefore, the influence of distance may easily lead to misclassification of a tensile event located away from the receiver, as a shear event located close to the receiver. It is evident, that any crack characterization scheme in real structures should include certain waveform correction procedures in order to lead to meaningful results. Concerning laboratory specimens which are commonly used for fracture characterization purposes, the effect of distortion is limited due to smaller dimensions and short propagation distances. However, as the results of the present study show, distortion does exist and although it does not prevent from the establishment of simple classification schemes, characterization would certainly benefit in terms of accuracy by taking out the effect of propagation distance.

The specific problem is quite complicated and further numerical and experimental efforts should be undertaken. Experiments of different fracturing modes should be conducted, while the number of sensors must be increased in order to monitor AE signals for longer distance. Concerning simulations, these should be expanded in three dimensions in order to more realistically simulate the exact geometry and orientation of the sensors' surface relatively to the AE wave directions.

Without being the target problem of the present study, a few comments can be pointed at the comparison between the AE parameters of different materials (plain and fiber reinforced). Apart from matrix cracking, failure in steel fiber materials includes another fracture mechanism due to the fiber pull-out. For the case of straight fibers when the material is being cracked, friction between the fibers and the surrounding matrix occurs, which resembles shear. As mentioned in the experimental section, the loading automatically stops at the first load drop; therefore, it is not possible to monitor sufficient number of pull-out events. However, it is certain that the fibers located at the center of the specimen are instantaneously involved in pull-out events when the main crack is formed. This contribution of the steel fibers' friction with the cement matrix is bound to be responsible for this slight increase of the average RA value for SFRM (371 μs/V) compared to 278 μs/V for plain mortar, as seen in Table 2 for sensor 1. For the same reason the AF is slightly decreased for SFRM. This has been experimentally seen in concrete studies [13,14,38] with extensive pull-out stage. In this case the contribution of pull-out is instantaneous, but still its influence is evident on the average values. On the other hand it is interesting to comment on the variation of the measurements, which is certainly higher for SFRM. Table 2 includes the standard deviation of the AE parameters as a percentage of the average. It can be seen that, especially for RA, the scatter of the different specimens is much higher for SFRM (approximately 50% compared to 30% or less for the plain material). This is also evident in Fig. 6b, where the scatter of experimental points is larger than Fig. 6a. This is particularly interesting because it shows that the increased inhomogeneity of the steel fiber material is reflected in

variability of the fracturing properties along with other physical properties, variability in which would be certainly expected.

7. Conclusions

The present study occupies with propagation of elastic wave pulses within material with microstructure. The investigation includes AE parameters which are used for characterization of the fracturing properties of materials, instead of the classical wave speed and attenuation which are related to mechanical and physical properties. These parameters are mainly average frequency and the inverse of the rising angle of the waveform (RA value) which under controlled conditions are used for crack classification purposes. Due to the heterogeneity of concrete, the waveforms are continuously distorted as the wave propagates away from the source. This results in significant shift of the original content when the pulses are recorded by the receiver. Experiments in specimens of mortar show that an additional propagation distance of a few cm affects the calculated values by orders of magnitude. RA increases by three to four times while frequency decreases by about 30%. This strong influence would not allow the use of any laboratory-based criterion in situ. Simulations were also conducted in order to expand to different materials and higher frequencies. They showed even higher influence of inhomogeneity on the propagating wave. Therefore, it is evident that the AE waveform as received by the sensor should not be directly used for crack classification purposes; instead the original waveform characteristics, as emitted by the crack, should be sought for in order to exclude the distortion that propagation in a heterogeneous medium induces.

Acknowledgment

The contribution of Dipl. Materials Engineer Pelia Giannoulatou in making and testing the mortar specimens is acknowledged.

References

[1] Grosse CU, Ohtsu M. Acoustic emission testing. Heidelberg: Springer; 2008.
[2] Mindess S. Acoustic emission methods. In: Malhotra VM, Carino NJ, editors. CRC handbook of nondestructive testing of concrete. Boca Raton (FL): CRC; 2004.
[3] Gudmundson P. Acoustic emission and dynamic energy release rate for steady growth of a tunneling crack in a plate in tension. J Mech Phys Solids 1999;47:2057–74.
[4] Carpinteri A, Cardone F, Lacidogna G. Energy emissions from failure phenomena: mechanical, electromagnetic, nuclear. Exp Mech 2010;50:1235–43.
[5] Moura A, Lei X, Nishisawa O. Prediction scheme for the catastrophic failure of highly loaded brittle materials or rocks. J Mech Phys Solids 2005;53:2435–55.
[6] Suzuki T, Ogata H, Takada R, Aoki M, Ohtsu M. Use of acoustic emission and X-ray computed tomography for damage evaluation of freeze-thawed concrete. Constr Build Mater 2010;24:2347–52.
[7] Kurz JH, Finck F, Grosse CU, Reinhardt HW. Stress drop and stress redistribution in concrete quantified over time by the B-value analysis. Struct Health Monit 2006;5:69–81.
[8] Shiotani T, Fujii K, Aoki T, Amou K. Evaluation of progressive failure using AE sources and improved B-value on slope model tests. Prog Acoust Emission 1994;7:529–34.
[9] Watanabe T, Hosomi M, Yuno K, Hashimoto C. Quality evaluation of shotcrete by acoustic emission. Constr Build Mater 2010;24:2358–62.
[10] Ohtsu M. Recommendation of RILEM TC 212-ACD: acoustic emission and related NDE techniques for crack detection and damage evaluation in concrete: test method for classification of active cracks in concrete structures by acoustic emission. Mater Struct 2010;43(9):1187–9.
[11] Yuyama S, Li Z, Ito Y, Arazoe M. Quantitative analysis of fracture process in RC column foundation by moment tensor analysis of acoustic emission. Constr Build Mater 1999;13:87–97.
[12] Soulioti D, Barkoula NM, Paipetis A, Matikas TE, Shiotani T, Aggelis DG. Acoustic emission behavior of steel fibre reinforced concrete under bending. Constr Build Mater 2009;23:3532–6.
[13] Aggelis DG, Shiotani T, Momoki S, Hirama A. Acoustic emission and ultrasound for damage characterization of concrete elements. ACI Mater J 2009;106(6):509–14.
[14] Grosse C, Reinhardt H, Dahm T. Localization and classification of fracture types in concrete with quantitative acoustic emission measurement techniques. NDT & E Int 1997;30(4):223–30.
[15] Aggelis DG. Classification of cracking mode in concrete by acoustic emission parameters. Mech Res Commun 2011;38:153–7.
[16] Shiotani T. Evaluation of long-term stability for rock slope by means of acoustic emission technique. NDT & E Int 2006;39(3):217–28.
[17] Anastassopoulos A, Philippidis TP. Clustering methodology for evaluation of acoustic emission from composites. J Acoust Emission 1995;13:11–22.
[18] Philippidis TP, Assimakopoulou TT. Strength degradation due to fatigue-induced matrix cracking in FRP composites: an acoustic emission predictive model. Compos Sci Technol 2008;68:3272–7.
[19] Scholey JJ, Wilcox PD, Wisnom MR, Friswell MI. Quantitative experimental measurements of matrix cracking and delamination using acoustic emission. Composites: Part A 2010;41:612–23.
[20] Ohtsu M, Tomoda Y. Phenomenological model of corrosion process in reinforced concrete identified by acoustic emission. ACI Mater J 2008;105(2):194–200.
[21] Lu Y, Li Z, Liao WI. Damage monitoring of reinforced concrete frames under seismic loading using cement-based piezoelectric sensor. Mater Struct 2011;44(7):1273–85.
[22] Ohno K, Ohtsu M. Crack classification in concrete based on acoustic emission. Constr Build Mater 2010;24(12):2339–46.
[23] Hamstad MA, O'Gallagher A, Gary J. A wavelet transform applied to acoustic emission signals: part 1: source identification. J Acoust Emission 2002;20:39–61.
[24] Aggelis DG, Matikas TE. Effect of plate wave dispersion on the acoustic emission parameters in metals. Comput Struct. doi:10.1016/j.compstruc.2012.01.014.
[25] Tsuda H, Koo J-H, Kishi T. Detection of simulated acoustic emission with Michelson interferometric fiber-optic sensors. J Mater Sci Lett 2001;20(1):55–6.
[26] Waterman PC, Truell R. Multiple scattering of waves. J Math Phys 1961;2:512–37.
[27] Chaix JF, Garnier V, Corneloup G. Ultrasonic wave propagation in heterogeneous solid media: theoretical analysis and experimental validation. Ultrasonics 2006;44:200–10.
[28] Punurai W, Jarzynski J, Qu J, Kurtis KE, Jacobs LJ. Characterization of entrained air voids in cement paste with scattered ultrasound. NDT & E Int 2006;39(6):514–24.
[29] Aggelis DG, Polyzos D, Philippidis TP. Wave dispersion and attenuation in fresh mortar: theoretical predictions vs experimental results. J Mech Phys Solids 2005;53:857–83.
[30] Kinra VK, Day NA, Maslov K, Henderson BK, Diderich G. The transmission of a longitudinal wave through a layer of spherical inclusions with a random or periodic arrangement. J Mech Phys Solids 1998;46(1):153–65.
[31] Tsinopoulos SV, Verbis JT, Polyzos D. An iterative effective medium approximation for wave dispersion and attenuation predictions in particulate composites. Adv Compos Lett 2000;9:193–200.
[32] Cowan ML, Beaty K, Page JH, Zhengyou L, Sheng P. Group velocity of acoustic waves in strongly scattering media: dependence on the volume fraction of scatterers. Phys Rev E 1998;58:6626–36.
[33] Yang L, Turner JA. Scattering of elastic waves in damaged media. J Acoust Soc Am 2003;113(6):2992–3000.
[34] Littles Jr JW, Jacobs LJ, Qu J. Experimental and theoretical investigation of scattering from a distribution of cracks. Ultrasonics 1995;33(1):37–43.
[35] Papargyri-Beskou S, Polyzos D, Beskos DE. Wave dispersion in gradient elastic solids and structures: a unified treatment. Int J Solids Struct 2009;46:3751–9.
[36] Aggelis DG, Shiotani T. Experimental study of surface wave propagation in strongly heterogeneous media. Journal of the Acoustical Society of America 2007;122(5):EL-151–7.
[37] EN 13892-2:2002. Methods of test for screed materials – part 2: determination of flexural and compressive strength
[38] Aggelis DG, Soulioti DV, Sapouridis N, Barkoula NM, Paipetis AS, Matikas TE. Acoustic emission characterization of the fracture process in fibre reinforced concrete. Constr Build Mater 2011;25:4126–31.
[39] Wave2000, Cyber-Logic. Inc. NY <http://www.cyberlogic.org>.
[40] Kaufman JJ, Luo G, Siffert RS. Ultrasound simulation in bone. IEEE Trans Ultrason Ferroelectr Freq Control 2008;55(6):1205–18.
[41] Uddin FAKM, Shigeishi M, Ohtsu M. Fracture mechanics of corrosion cracking in concrete by acoustic emission. Meccanica 2006;41:425–42.
[42] Moser F, Jacobs LJ, Qu J. Modeling elastic wave propagation in waveguides with finite element method. NDT & E Int 1999;32:225–34.